# CrystEngComm

Accepted Manuscript






ROYAL SOCIETY OF CHEMISTRY

www.rsc.org/crystengcomm

# Controlled (110) and (101) crystallographic plane growth of single crystalline rutile $TiO_2$ nanorods by facile low cost chemical methods

**P. Soundarrajan,[a] K. Sankarasubramanian,[a] K. Sethuraman*[a] and K. Ramamurthi[b]**

[a]*School of Physics, Madurai Kamaraj University, Madurai 625021, Tamil Nadu, India*

[b]*Department of Physics and Nanotechnology, SRM University, Chennai 603203, Tamil Nadu, India*

## Abstract

A new approach has been employed to grow large size and number dense rutile $TiO_2$ nanorods (NRs) by low cost chemical methods. The low (~30 nm) and high (~150 nm) thickness of nuclei layers have been optimized on glass substrate for growing NRs using spin coating and chemical spray pyrolysis method respectively. The scanning electron and atomic force microscopic images clearly exhibit that the randomly aligned large size exotic NRs have grown on low thickness seed layer at higher temperature (180 ºC) and interconnected well number dense NRs have grown on high thickness seed layer at lower temperature (120 ºC) via hydrothermal synthesis. The structural studies clearly reveal that the as-grown NRs are tetragonal rutile structure with different anisotropic crystallographic plane growth along c-axis. The preferentially oriented (110) Bragg reflection in large size NRs and (101) Bragg reflection in number dense NRs illustrate that the Ti atoms are positioned in the middle of atomic layer and stimulate randomly standing NRs along the direction of stacking. The growth orientation and single crystalline nature of the NRs are strongly confirmed by high resolution transmission electron microscopic technique and μ-Raman scattering. The absorbance value and shift in UV-vis energy region of electron of $TiO_2$ NRs are strongly dependent on the number density and/or size of the NRs. The crystal defects of prepared rutile $TiO_2$ NRs are analyzed using photoluminescence spectra. Our

results represent that the thickness of the seed layer and growth temperatures are played a pivotal role for determining the two anisotropic crystallographic plane growths of rutile $TiO_2$ NRs.

**Key words:** Spin coating; spray pyrolysis; $TiO_2$ seed layer; hydrothermal; crystal growth; structural and optical properties.

***Corresponding author**

**Dr. K. Sethuraman,**

**School of Physics,**

**Madurai Kamaraj University,**

**Madurai – 625 021, Tamil Nadu, India,**

**E-mail:sethuraman_33@yahoo.com, Mobile no: +919445252309**

## 1. Introduction

$TiO_2$ is a large energy band-gap (~3.2 eV, 2p levels of $O^{2-}$ valence band to 3d levels of $Ti^{4+}$ conduction band) semiconductor and is widely investigated for its use in both energy and environmental applications such as self-cleaning, photocatalyst and photoelectrode in liquid junction solar cells owing to their strong oxidizing capacity, nontoxicity, and long-term photostability.[1-8] In particular, the synthesis of $TiO_2$ nanomaterial demonstrates high performance levels for these applications when compared to their bulk form due to their higher surface to volume ratio. Especially, one dimensional (1D) $TiO_2$ nanostructures such as nanorods (NRs), nanowires (NWs), and nanotubes (NTs) have accelerated research on nanoscale materials because of their well-defined crystalline structure, unique optical properties and quantum

confinement effect. These excellent properties provide ideal electron transport during cell performance, which minimize the charge recombination process.[9-14]

Nanostructures of $TiO_2$ can exist in three crystal structures such as two tetragonal forms: anatase, rutile, and one rhombic form: brookite. Among them, the (110) surface of rutile $TiO_2$ is showing to be highly active for photocatalytic water splitting and numerous other applications in photochemistry and catalysis.[15, 16] The rutile form of NRs is mainly surrounded by the (110) crystallographic plane and that is thermodynamically most stable surface at ambient conditions. Therefore, growing the particular surface orientation of rutile $TiO_2$ film is important. Further, the size and shape of the NRs is mainly depends on the synthetic conditions.

Several techniques such as sputtering,[17] MOCVD,[18] aerosol pyrolysis,[19] electro deposition,[20] sol-gel method,[21, 22] spray pyrolysis[23] and hydrothermal[24, 25] have been adopted for the preparation of $TiO_2$ nanostructured thin films. Among these diverse conventional techniques, hydrothermal synthesis is a simple and cost effective method for growing well-aligned nanostructures with high specific surface area and, the single-crystalline material is easily obtained.[26, 27] Also, the particle size, morphology and structure are mainly depends on the preparation parameters such as pH, temperature and so on. On the other hand, well-known chemical routes such as spin coating, chemical spray pyrolysis, dip coating and physical methods such as electron beam evaporation have been employed for seed layer preparation.[22, 23, 28] Among them, spin coating and chemical spray pyrolysis technique can act as promising techniques to deposit uniform coatings of materials on high-aspect ratio structures with less thickness. Another benefit of these methods is well known low cost methods because of no need of any expensive equipment.

The aspect ratio and length of the NRs are very important for the applications perspective. The reason is surface to volume ratio of the NRs dependent on the aspect ratio of the NRs. Hence, it is expected that the aspect ratio of the NRs might be one of the most promising for deciding carrier transport in electronic devices. Further, the length of the NRs leads to the formation of single-crystalline nature and also enhancing the electron transport. The aspect ratio and length of the NRs can be easily controlled by the synthetic conditions such as growth temperature, precursor concentration, pH of the solution and growth time. C. Wang et al. have investigated how the crystal size and shape of the $TiO_2$ NRs could be adjusted by varying solution conditions. The diameter and density of the NRs are directly proportional to the precursor concentration. Further, the NRs diameter increased dramatically with respect to change in volume of the DD water and HCl. Finally, it was concluded that the length and diameter with constant spacing of the NRs of working electrode give the maximum power conversion efficiency in quantum dot sensitized solar cell.[26] H. Wang et al. have reported fabrication of single-crystalline NRs on conductive substrate (FTO) by hydrothermal synthesis for application in quantum dot sensitized solar cells. The NRs are nearly perpendicular to the FTO substrate with respect to preferentially oriented (002) crystallographic plane. The length is up to 3 μm. The shrinkage of NRs along the growth direction at acidic medium leads to the formation of single-crystalline nature.[27] A. Wolcott et al. have fabricated dense and aligned NRs arrays using oblique-angle deposition on FTO substrate. The number density of the NRs is in the order of $25x10^6/mm^2$ and it is also expected to be useful for photoelectrochemical cells applications.[29] J. T. Park et al. have grown the vertically aligned $TiO_2$ NRs with high density on spin coated seed layer covered FTO glass. The NRs are homogeneously distributed on the substrate with length of 3 μm and diameter of 70 nm.[30]

From the above articles survey, we realized that the quality of the NRs is very important for device applications. Hence, here, we have devoted to prepare $TiO_2$ nuclei layer on bare glass substrate using two deposition techniques such as spin coating and chemical spray pyrolysis. $TiO_2$ seed layer coated glass substrates subjected to heat treatment (annealing) at 450 ºC for 4 h to improve their crystallinity. Further, the hydrothermal synthesis is used to growing $TiO_2$ NRs on seed layer coated glass substrates. Extensive investigations have been carried out to understand the growth of NRs and phase transformation of $TiO_2$ nanostructures on seed layer coated glass substrates.[31-35]

Presently, we have optimized, for the first time, minimum and maximum thickness of seed layer on glass substrate by two chemical deposition methods for growing 1D rutile $TiO_2$ NRs under two different growth temperatures (180 and 120 ºC). The NRs are randomly grown along c-axis with two different preferentially oriented crystallographic planes, which stimulate the lengthy and number dense NRs. This approach is new and not seen in the literatures.

## 2. Experimental Section

Titanium (IV) isopropoxide (TTIP) 95% was used as a source material for titanium (Ti) and purchased from Sigma-Aldrich. Ethanol, double distilled (DD) water and acetic acid were used as solvent and stabilizing agent respectively. Further, the hydrochloric acid (HCl) served as an acidic catalyst to control the hydrolysis rate of the titanium source. The ethanol, acetic acid and HCl were obtained from Merck and used as received. Microscopic glass slides of the dimension 37.5 mm x 12.5 mm x 1 mm were used as substrates. The substrates were washed using soap solution and subsequently kept in hot chromic acid at 70 ºC for 30 minutes and then cleaned in double distilled water and acetone separately in an ultrasonic bath.

The first $TiO_2$ seed layer was prepared by sol-gel spin coating method. The appropriate amount of TTIP, 18 ml of ethanol, and 0.2 ml of acetic acid were mixed together and stirred for about 2 h at room temperature to get final sol-gel solution. The prepared sol-gel solution was dropped onto the well cleaned glass substrate. It was rotated at a speed of 3000 rpm for 30 s resulting in the formation of thin layer film. The number of samples was prepared with respect to change in preparatory parameters. The films were baked at 100 ºC for 10 min and then allowed to reach ambient temperature. Subsequently, the baked films were annealed at 450 ºC in a muffle furnace at a constant heating rate in the air atmosphere for about 4 h.

Another $TiO_2$ seed layer was deposited on a bare glass substrate by chemical spray pyrolysis technique. TTIP was added drop by drop into ethanol with continuous vulnerable stirring. The transparent resultant precursor solution was obtained after 30 min. The resultant final solution was sprayed through the nozzle onto the preheated glass substrate at 200 ºC with the help of air compressor. The spray pyrolysis parameters such as substrate temperature and precursor concentration were changed to prepare more than five samples and other parameters kept constant such as spray angle, spray time and spray interval. The prepared $TiO_2$ seed layer films were annealed at 450 ºC for 4 h.

The $TiO_2$ NRs were grown on seed layer coated glass substrates by hydrothermal method. The appropriate amount of HCl (35%) was mixed with double distilled water and stirred for 10 min. 0.2 ml of TTIP solution was added drop by drop to the above solution. The final precursor solution was transferred into a Teflon lined stainless steel (50 ml capacity) autoclave. The $TiO_2$ NRs were grown on the seed layer coated substrate inclined at 45º to the walls of Teflon with its face up. Hydrothermal process was carried out at 120 ºC for 16 h on spray coated seed layers and 180 ºC for 4 h on spin coated seed layers. Further, the some of the spray pyrolysis coated nuclei

layer films was introduce to NRs growth at temperature of 120 ºC – 180 ºC within the growth time 4-16 h. After hydrothermal synthesis, the autoclave was left to reach room temperature. The substrate was taken out from the solution, continuously, dried at room temperature. Before going to take characterization, we have named as a and b for spin and spray pyrolysis coated nuclei layer and $TiO_2$ NRs grown on the corresponding seed layer is denoted as $a_1$ and $b_1$.

Crystalline phase and growth direction of $a_1$ and $b_1$ NRs were determined using a Brucker D8 Advance X-ray diffractometer (XRD) [$2\theta$ = 10-80˚, CuK$\alpha$ = 1.540 Å]. Single crystalline nature of the NRs was confirmed by high resolution transmission electron microscopy (HRTEM) (PHILIPS, model – CM200, operated at 200 kV accelerating voltage). The surface morphology of the $a_1$ and $b_1$ NRs was analyzed by a JEOL (JSM – 5610LV) scanning electron microscopy (SEM). The surface topography and RMS surface roughness of a, b and $a_1$, $b_1$ samples were examined by atomic force microscopy (AFM) (Non-contact mode, A100 SGS, APE Research). The optical absorption spectra of a, b and $a_1$, $b_1$ samples were recorded in the wavelength range of 190-900 nm using shimadzu-UV 2450 double beam spectrophotometer at room temperature. The photoluminescence spectra of the $TiO_2$ NRs were analyzed by RF – 5301 spectroflurometer in the wavelength range of 300-800 nm. The vibrational properties of $TiO_2$ NRs were analyzed by Fourier transforms infrared spectra (FTIR) (BRUKER Optik) in the wave number range of 400 – 4000 $cm^{-1}$. A spot size of ~1µm $a_1$ and $b_1$ NRs were excited using 632.8 nm He-Ne laser line from LabRam HR800 micro-Raman instrument and recorded its backscattering mode in the wave number range of 100-800 $cm^{-1}$.

## 3. Results and Discussion

### 3.1 Structural and morphological studies of $TiO_2$ NRs

Fig. 1 depicts the X-ray diffraction pattern of the $a_1$ (2θ=10-80º) and $b_1$ (2θ=15-75º) NRs. The XRD of the as-grown NRs on spin coated seed layer is consisting of diffraction peaks at 2θ values of 27.4º, 36.1º, 39.1º, 41.2º, 44.0º, 54.3º, 56.6º, 63.0º and 69.8º due to the (110), (101), (200), (111), (210), (211), (220), (002) and (112) Bragg reflections. All the diffraction peak of NRs is corresponding to a pure crystalline tetragonal rutile phase (JCPDS no 76-0317, a = 4.592, b =2.957). Some of the Bragg peaks in X-ray pattern indicate the strong orientation along a specific direction. The relatively intense diffraction peak at 2θ = 27.4º corresponding to (110) plane indicates the preferential orientation growth along c-axis. Narrow full width at half maximum (FWHM) of tall (110) diffraction peak (~0.142) demonstrates that the NRs are strong rutile phase and good crystalline quality. The {001} facets exposed rutile structure of the individual $TiO_2$ NRs are sustained by repeating (110) crystallographic plane side surface along the direction of stacking. No characteristic peak was observed for other polymorphs which indicate the high purity and single phase crystalline nature of the rutile $TiO_2$ NRs. The crystallite size of the $a_1$ sample estimated by scherrer formula and it is found to be ~52 nm. The $TiO_2$ NRs grown on chemical spray pyrolysis coated seed layer show diffraction peaks at 2θ values of 27.4º, 36.1º, 41.2º, 54.3º and 63.0º due to (110), (101), (111), (211) and (002) diffraction planes of tetragonal rutile structure (JCPDS 76-0317). One extra peak observed at 25.4º due to (101) plane corresponding to anatase phase (JCPDS 86-1285). The XRD of as-grown NRs on spray pyrolysis coated nuclei layer is well-matched with the reported article, where the dense rutile NRs were grown on anatase seed layer by the help of (101) crystallographic direction.[28] XRD pattern of $b_1$ sample shows the predominant Bragg reflection at 36.10º with FWHM of 0.176, which is an indication of smaller crystallite size. The half-width of the (110) Bragg reflection is sharper than the (101) Bragg reflection, which indicates that the film grows anisotropically. A

contact angle between the (101) and (002) crystallographic plane is ~33º. Hence, here some of the NRs are perpendicular to the substrate surface, while another NRs lean towards the azimuthal direction. The presence of anatase Bragg reflection reveals that the edge-shared bonding formed on the anatase nuclei particles at the initial stage of the hydrothermal reaction owing to lattice mismatch with respect to lower growth rate. Therefore, the preferentially oriented crystallographic plane growth of 1 D $TiO_2$ nanostructures can be affected the physical, chemical, and electrical properties. Further, the mechanical strength of the material is also affected.

In theoretical prediction, the four types of two dimensional titania slabs such as (110), (100), (101) and (001) generated one-dimensional rutile $TiO_2$ nanostructures[36] because the growth rate of these different crystal faces depends on the numbers of corners and edges of the coordination polyhedra available. Compare with other polymorphs, rutile $TiO_2$ polymorph has higher surface energy. But, the experimentally Ti-HCl ratios in the solution determine the particular phase growth of $TiO_2$ nanostructure. The fixed precursor concentration leads to the formation of rutile crystallite on the anatase seed layer substrate. In our case, the rutile $TiO_2$ NRs are grown on different thickness of nuclei layer under hydrothermal reaction at lower (120 ºC) and higher (180 ºC) temperature. Hence, the different growth rate is expected in this work. At higher solution temperature, the (110) crystallographic plane could be exposed on low thickness seed layer under higher growth rate owing to its higher surface energy. Here, the atoms are exposed to form (110) crystallographic plane at higher temperature by a fourfold-coordinated Ti atom and 2 twofold-coordinated oxygens of the first layer, as well as fully coordinated oxygen of the second layer. This is the main reason for (110) crystallographic plane growth of rutile $TiO_2$ has most stable surface. On another hand, the reactant system energy is directly proportional to the temperature of the autoclave. Therefore, the system energy is decreases when the lower growth temperature.

At lower growth temperature, the (101) preferentially oriented crystallographic direction is induced on high thickness seed layer with respect to lower growth rate. Both fivefold- and sixfold- coordinated Ti atoms as well as twofold and threefold oxygens are stimulated to form (101) crystallographic plane growth of rutile $TiO_2$ NRs at lower growth temperature. The preferentially oriented crystallographic (110) plane in $a_1$ and (101) plane in $b_1$ NRs are parallel to the NRs growth direction (inset – XRD). This result reveals that the rutile NRs are standing randomly along the c-axis. The careful selection of the initial nucleation by nuclei layer thickness and control of Ti growth ratio by growth temperature are deciding the different preferentially oriented crystallographic plane growth of rutile $TiO_2$ NRs. Hence, we conclude that the seed layer thickness and growth temperature have influence on the internal factor of energetically favorable surface, thus lead to the formation of (110) and (101) crystallographic planes.

The crystallinity and growth direction of the $a_1$ and $b_1$ NRs were then confirmed by TEM, HRTEM and SAED characterization. Fig. 2 (i-iii) and (iv-vi) represent the $a_1$ and $b_1$ NRs TEM, HRTEM and SAED patterns. The $a_1$ NRs lattice fringes with an interplanar spacing parallel to the side wall is ~0.311 nm, in accordance with the (110) crystallographic planes of tetragonal rutile $TiO_2$ structure. TEM image of the $b_1$ sample clearly reveals that the bunch of small NRs pillars agglomerate to form NRs. The lattice fringes with an interplanar spacing perpendicular to the side wall is ~0.290 nm, in accordance with the {001} facets and is quite apparent from the HRTEM fringes. The SAED patterns of the both NRs provide more evidence for the c- axis orientation growth and single crystalline nature of rutile $TiO_2$ NRs. This result provides a strong confirmation of the tetragonal rutile structure of $TiO_2$ NRs and it is consistent with the XRD results.

The SEM images of as-grown $TiO_2$ NRs denoted as $a_1$ and $b_1$ are shown in Fig. 3. Two thicknesses of seed layers prepared using two chemical methods such as spin coating and chemical spray pyrolysis for NRs growth. During hydrothermal reaction, the orientation, size and shape of the NRs mainly depends on the growth time, growth temperature, substrate, reactant concentration and acidity. But, here, the two different preferentially oriented crystallographic plane of rutile NRs grow significantly on different size of nuclei (it depends on the thickness of nuclei layer) under different growth temperature. The NRs are found to be homogeneously distributed overall the substrates, which indicate that the preparation methods are very important to deposit large area production by low-cost. The evolution of the various preferentially oriented crystallographic plane of 1D NRs on different thickness nuclei layers under two various growth temperature is discussed.

It is well known that the growth rate is strongly depends on the growth temperature within the autoclave. Therefore, the growth rate is fast in the higher growth temperature and thus leads to the formation of lengthy rutile $TiO_2$ NRs with respect to (110) preferentially oriented diffraction plane. The length and diameter of the NRs is ~ 1.5 μm and 600 nm respectively and are shown in the Fig. 3($a_1$). The diameter of the NRs is shrinking, when the NRs growth along the c – axis. The reason is rapid growth of (001) crystallographic plane under coarsening mechanism significantly reduces the surface energy, especially in the acidic medium. The density of the NRs is calculated approximately to be $3 \times 10^4$ $cm^{-2}$. Fig. 3($b_1$) exhibits the SEM images of as-grown rutile $TiO_2$ NRs on chemical spray pyrolysis coated seed layer. At lower solution temperature, the growth rate is slow in the system which stimulates number dense randomly aligned NRs with the help of (101) crystallographic plane on high thickness nuclei layer. For clear identification of number dense NRs, 1 μm and 500 nm scale bar SEM images are used. The average diameter and

length of NRs are 150 and 600 nm respectively. From low magnification SEM image, the flower like NRs are observed randomly on nuclei layer owing to large size of nuclei would be presented in some region of high thickness seed layer. The density of the number dense NRs is found to be approximately 2.4 x $10^5$ $cm^{-2}$. Therefore, number dense of the NRs is being observed at lower growth temperature (120 ºC) and the low density with large size of NRs are seen in the higher temperature of 180 ºC. Generally, the low growth rate is induced number dense NRs with respect to collision between ions in the medium at lower temperature. The solution pressure decides the collision between ions and is directly proportional to the temperature of the solution in the hydrothermal process. In our study, it is found that the number density and large size of the $TiO_2$ NRs could be grown by varying solution temperature as well as seed layer thickness. The number dense NRs can offer a larger surface area for dye adsorption and large size NRs gives opportunities for higher amount of quantum dots sensitizing. Therefore dye molecule or QDs interpenetration with 1 D metal oxide working electrode in liquid junction solar cell is a key factor for photocurrent generation and it is critically dependent on the size and/or number density of NRs.[26] The aspect ratio $\alpha$ ($\alpha$= length/width) of the (110) and (101) preferentially oriented $a_1$ and $b_1$ NRs is found to be approximately same with square top. Fig. 3($a_2$, $b_2$) illustrate the square top diameter distribution of $a_1$ and $b_1$ NRs, which ensures that the $TiO_2$ NRs in the form of tetragonal crystal structure. Extensive investigation reported that the rutile NRs were made up from agglomeration of small number of NRs. Here, we report well defined tetragonal shaped rutile NRs without coalescence of small NRs pillars particularly in $a_1$ sample, which is beneficial for effective flow of electrons in the optoelectronic devices. The size of the nuclei particles depends on thickness of seed substrate and it is determining the diameter of the growing $TiO_2$ NRs. The reason is size of the nuclei confine the diameter and promote the randomly aligned

NRs along the c – axis. Further, during the initial NRs growth, diameter of the nuclei is restricted by the neighboring nuclei nanoparticles. Ti and O atomic layers are stacked alternatively, which decides the number dense and lengthy NRs under preferentially oriented crystallographic plane with respect to growth rate and size of the nuclei. Hence, the present work has opened a new experimental procedure for producing number dense and number dense free lengthy rutile $TiO_2$ NRs.

An energy dispersive X-ray spectroscopy (EDAX) analysis, which offers information about the elemental composition, collected during SEM analysis. EDX spectrum was recorded with the accelerating voltage and the working distance of 10 kV and 8 nm respectively. Fig. 4 shows the EDX spectrum of the top portion of single NRs $a_1$ sample. Here, we have recorded the EDX spectra from the magnified top view and hence carbon and copper signals come from double-sided carbon tape and copper stub, respectively. Some of the NRs randomly standing on seed layer glass substrate, therefore, the stoichiometry of the Ti and O are probed at three points (~bottom, middle and top) along the axial direction by selecting the option 'point & id' from the top view. The oxygen peak at 0.5 keV (O Kα) indicates that the O is dominant and the Ti peaks at 4.5 keV (Ti Kα) and 4.9 keV (Ti kβ) are observed in signal coming from the bottom, middle and top portion of the single nanorod. The $TiO_2$ NRs grown on spin coated seed layer have Ti and O ratios in the bottom, middle and top portion of the NRs are 30.78:60.22, 30.94:60.06 and 30.13:60.87 at.% respectively and 30.62:60.38, 30.69:60.31 and 30.00:60.00 at.% for $TiO_2$ NRs grown on spray pyrolysis coated seed layer. EDX analyses clearly revealed that the main bodies of 1D $TiO_2$ NRs consist of Ti and O. This result is well collaborate with the literature value.[31] Uniform and well adherently coated $TiO_2$ NRs films photographs are shown in the inset of $a_1$ EDX spectrum.

2D AFM images of a, b seed layers and 2D, 3D AFM images of $a_1$, $b_1$ NRs are shown in the Fig. 5. After few attempts and careful selection of spot area, we have taken AFM images for $a_1$ and $b_1$ NRs. The seed layers a and b reiterate that the high density nuclei nanoparticles are uniformly distributed on the bare glass substrates as well as some voids are observed in the samples. This nucleation center is supporting for the subsequent growth of NRs with respect to lower interface energy between the crystal nuclei and the substrate. Thicknesses of the seed layers and height of the NRs measured using stylus profilometer and height profile of AFM. The height of the NRs is ~1.5 μm and 600 nm for $a_1$ and $b_1$ NRs respectively. 2D and 3D AFM images of the $a_1$ sample depict the NRs are randomly distributed and not interconnected well and hence we suggest that the formation of lengthy and number dense free NRs on low thickness seed layer. The densely packed NRs are observed in 2D and 3D AFM images of $b_1$ sample. The interconnected well without coalescence of NRs provides evidence for the formation of number dense NRs on high thickness seed layer. The AFM images of NRs are well corroborating with the SEM images.

**3.2 Optical studies of $TiO_2$ NRs**

The compound semiconductors such as metal oxides and metal chalcogenides have both ionic and covalent bonds between atoms, which can induce energy band gap in the materials. Recording the absorption spectrum for semiconductor is directly determining the electronic structure of the material by stimulates electron from the valence band to the conduction band using ultraviolet and visible region of energies. Hence, the UV-vis photons are passed through the $TiO_2$ seed layers and NRs and recorded in the wavelength range of 190 – 900 nm. The optical absorbance spectra of the $TiO_2$ NRs and seed layer films in the range of 300-450 nm are shown in the Fig. 6(i). From the Fig. it is clear that the strong light response in the UV region can be

attributed to band-band transitions, which is characteristic of the wide band-gap $TiO_2$ nanostructures. The redshift in absorption of the $TiO_2$ NRs as compared to the seed layer coated glass substrate owing to increasing thickness/length of the NRs. It illustrates the better light trapping effect of $TiO_2$ NRs. Further, compared with $b_1$, the $a_1$ NRs is red shifted, which is due to the increase in crystallinity. The marginal change in absorbance value of $TiO_2$ NRs may be attributed to the difference in number of NRs on the seed layer coated glass substrates. It elucidate that the light trapping effect of 1D $TiO_2$ NRs is directly proportional to the number dense of NRs. Fundamentally, $TiO_2$ possesses an indirect bandgap system and the band-gap energies of NRs were calculated using Tauc's plot $E_g = (\alpha h\nu)^{1/2}/(h\nu)$ (Fig. 6(ii)) method. Where, $h\nu$, $\alpha$ and $E_g$ are the photon energy, absorption coefficient and band gap of the inter-band transition respectively. The observed linear behavior in the energy region is corresponding to a strong absorption near the absorption edge. Extrapolating straight line from the linear portion of the curve to zero absorption edge gives the bandgap of the NRs. In addition, the energy gaps for the rutile and anatase $TiO_2$ nanostructures are 3.0 and 3.3 eV respectively.[28] The calculated bandgap values of high density nanoparticles contained anatase seed layers and rutile NRs are in good agreement with the reported literature values and the bandgap values of seed layers and rutile NRs are 3.21, 3.17 and 2.95, 3.01 eV respectively. The weak optical absorption in $a_1$ and $b_1$ NRs above the absorption edge wavelength region result from the sub-band transitions closely related to the surface oxygen vacancies (SOVs).

Crystallization quality and defect structures (charge carrier trapping, migration and transfer, and electron-hole pairs) of semiconductor materials are observed from photoluminescence spectrum (PL). The as-grown $TiO_2$ NRs are excited with the wavelength of 325 nm and the corresponding recorded emission spectrum in the wavelength range of 340-550 nm is shown in

Fig. 7(i). Generally, two emission bands are observed for $TiO_2$ nanostructure at room temperature. These emissions are classified into near band edge emission (NBE) and deep level emission (DLE). The NBE is due to radiative recombination of electrons from the conduction band to the valence band (band-to-band transition, $O_{2p}$ to $Ti_{3d}$). The stronger deep level emission in the visible region is mainly originated from defect states such as Ti interstitials and oxygen vacancies. In the as-grown $TiO_2$ NRs, the emission spectrum shows relatively broad visible emission but weak and intense NBE in the near UV region with FWHM of ~5 and 6 nm for $a_1$ and $b_1$ NRs respectively. The visible emissions erupt from the $a_1$ and $b_1$ NRs can be attributed to the (1) charge transfer transition from an oxygen vacancy trapped electrons and (2) Ti vacancies trapped electrons and then (3) SOVs. Generally in metal oxides, the vacancies neither metal nor oxygens and SOVs create deep levels below the bottom of the conduction band. The charge state of vacancies can drop one or two electrons to the valence band and depletion region which can induce considerable variation in the band gap.[37] The erupted emission around 415 and 483 nm is related to the SOVs, which is in good agreement with the absorption spectrum. Another emission peak at 451 nm is mainly attributed to the $Ti^{3+}$ vacancies. Although, 3D AFM images of $a_1$ and $b_1$ NRs clearly show that the air gap between randomly aligned lengthy NRs is high, compare with number dense NRs and this is the reason for lower recombination rate in $b_1$ sample. Therefore, the photo – excited emission is generating wide spectrum at a wavelength range of 400 to 550 nm, when the excitation photon travels through the air gap between the randomly aligned NRs and interact with the seed substrate. Hence, the SOVs are observed from the PL spectrum of $a_1$ and $b_1$ NRs. The NBE and DLE peak intensity of NRs depend on the air gap between each NRs and number density of NRs. The optical quality of the $TiO_2$ NRs confirmed

from near band edge emission peaking at 381 and 383 nm for $a_1$ and $b_1$ NRs respectively, and the stable SOVs are also confirmed by NRs excited with different wavelength photons.

Fig. 7(ii) shows FTIR transmittance spectrum of $a_1$ and $b_1$ NRs in the wavenumber range of 400-700 $cm^{-1}$. The $TiO_2$ NRs grown on spin coated seed layer and their transmittance peaks are 523 $cm^{-1}$, 504 $cm^{-1}$, 480 $cm^{-1}$, 448 $cm^{-1}$ and 418 $cm^{-1}$, which are assigned to the Ti-O-Ti stretching vibration in the rutile phase. The transmittance peaks of $TiO_2$ NRs grown on spray coated seed layer are 542 $cm^{-1}$, 474 $cm^{-1}$ and 428 $cm^{-1}$, which are assigned to the Ti-O-Ti stretching vibration in the tetragonal phase (rutile and anatase). No impurity peaks are detected in $TiO_2$ NRs.

μ-Raman measurement is being popularly used for the investigation of various phases of $TiO_2$ nanostructures. This technique is capable of elucidating the structural complexity of $TiO_2$ in which, the each phases (rutile or anatase) are easily distinguishable. The rutile $TiO_2$ phase is belongs to the tetragonal structure and exhibits symmetry characteristic of the space group $P4_2/mnm$. Each lattice contains 10 optical phonons of symmetries as there are 2 molecules per unit cell and expressed as $A_{1g} + A_{2g} + A_{2u} + B_{1g} + B_{2g} + E_g + 2B_{1u} + 3E_u$ and which are classified into three modes of vibration such as Raman-active, IR-active and inactive in both Raman and IR spectra respectively. The (110) and (101) crystallographic plane growth of tetragonal rutile nanostructures have two $TiO_2$ units (=O-$Ti_2O_2$-O= for (110) and =$O_2$-$Ti_2$-$O_2$= for (101)) per cell and have four Raman active modes. Experimentally, the Raman peaks appear at 235, 443, and 610 $cm^{-1}$, which assigned to the $B_{1g}$, $E_g$, and $A_{1g}$ modes of rutile $TiO_2$ respectively[38] and clear Raman bands at 244, 323, 442 and 607 $cm^{-1}$ are characteristic vibrations of rutile $TiO_2$.[39] The strong Raman peaks intensity at 450 and 610 $cm^{-1}$ for rutile $TiO_2$ nanocrystalline film reported by Ma et al.[34] The oxygen vibrational mode ($E_g$) and vibration mode of Ti-O bond ($A_{1g}$) of rutile

$TiO_2$ NRs show a slight red-shift in peak position and broader line width while comparing to bulk crystals, which are attributed to both phonon confinement and residual stress.[40, 41]

From the above Raman measurements review, we realize that the μ-Raman scattering is a powerful technique to analyze the $TiO_2$ material quality, phase orientation and single crystalline nature. Our prepared well adherent as-grown NRs denoted as $a_1$ and $b_1$ NRs subjected to μ-Raman scattering at room temperature. The recorded representative Raman spectra are shown in the Fig. 8. The Raman peaks observed at 143, 237, 446 and 610 $cm^{-1}$ on spin coated nuclei and 244, 323, 442, and 607 $cm^{-1}$ on spray pyrolysis coated nuclei are closely matched with the reference values, indicating that the as-grown $TiO_2$ NRs are in rutile form. The Raman band at 144 $cm^{-1}$ in $TiO_2$ NRs grown on spray pyrolysis coated nuclei layer is evidence for the presence of anatase phase. This result is well consent with the XRD result. The Raman band at 246 $cm^{-1}$ is due to the second order scattering by compound vibration, which is also considered as a characteristic vibration of rutile. It was reported that the thin film thickness determined the FWHM value of Raman modes in rutile $TiO_2$ nanostructure.[42] In our case, as-grown, single-phase $TiO_2$ NRs have large size and number density under synthetic conditions, thus leads to different surface to volume ratio of NRs. The FWHM of $E_g$ mode is calculated to be 41.99 and 47.13 $cm^{-1}$ for $a_1$ and $b_1$NRs respectively. Moreover, FWHM of $A_{1g}$ mode corresponding to the Raman band at 610 $cm^{-1}$ is calculated to be 40.20 and 53.43 $cm^{-1}$ for $a_1$ and $b_1$ NRs, respectively, indicating an increase in FWHM. The decrease of FWHM in $a_1$ sample indicates that the crystallinity is enhanced when NRs grown at higher temperature. These values are in good agreement with the results of XRD and SEM images. From $E_g$ and $A_{1g}$ Raman modes, the Raman peaks of the number dense NRs becomes broader, the reason is small size of NRs in $b_1$ sample

NRs gives higher degree of structural disorder. Further, the rutile $TiO_2$ single crystal is also confirmed by two prominent Raman bands such as $E_g$ and $A_{1g}$.

**4. Discussion and growth mechanism**

The mechanism for the observed two different preferentially oriented plane growth of rutile $TiO_2$ NRs on the anatase high density nanoparticle nuclei layer can be explained by the results of present study with literature survey.

1D nanostructured metal oxide have charge carrier transport many times faster than that of nanoparticles owing to their higher diffusion coefficient. Therefore, in order to develop $TiO_2$ based nanoscale functional devices, the controlled and quality of 1D nanostructure are essential. While developing 1 D nanotechnology, the 1 D $TiO_2$ nanostructures were mainly synthesized by researchers via physical deposition techniques including sputtering and chemical vapor deposition, where the vapor-liquid-solid (VLS) and vapor-solid (VS) transformation approaches at higher temperature. The resulting nanostructures are sensitively depending on preparatory conditions. [43] Mass production using physical methods are expensive. Owing to this reason, wet - chemical methods are attracted by nanotechnologist and this method is user – friendly and more suitable for inexpensive mass production. B. Liu et al. grew, for the first time, single-crystalline rutile 1 D $TiO_2$ NRs directly on FTO substrate using the hydrothermal method and the size and number density of $TiO_2$ NRs could be varied by changing the solution parameters.[31] This report has opened a new door for producing 1 D nanostructure on conductive substrate by low price for devices making. The nuclei layer including ITO and FTO substrates used for 1 D nanostructures growth, because of, thus far, bare glass substrate is unsuccessful one for 1 D nanostructures growth. The reason is lattice mismatch between nuclei particle and rutile $TiO_2$ is mainly considered during the growth of 1D nanostructure. Further, it was noticed that the resistivity

value of the FTO substrate determines the 1D nanostructure.[44] Finally, it is found that the role of thickness of seed layer on 1D $TiO_2$ NRs not seen in the research articles. The reason is conundrum to grow oriented anisotropic single - crystalline 1D nanostructure on seed particle layer coated bare glass substrate. The seed layer thickness is a pivotal factor because of it provides nucleation force and residual strain during the NRs growth. Therefore, after few months literature surveys, we planned to work in 1D $TiO_2$ NRs. First, we have deposited more than ten seed samples with various thicknesses using chemical spray pyrolysis and spin coating to optimize the growth conditions for growing 1D NRs. The minimum and maximum thickness of nuclei layer have been optimized by spin coating and chemical spray pyrolysis technique respectively. Approximately 30 nm of $TiO_2$ seed layer prepared by spin coating and 150 nm of $TiO_2$ seed layer prepared using spray pyrolysis technique are the optimum thicknesses for growing $TiO_2$ NRs. Two chemical deposition methods have been used to prepare seed layer the reason is evaluating low-cost methods to industrial people.

Hydrothermal synthesis under acidic conditions can be used to produce rutile nanocrystallites on anatase seed nanoparticles. Hence, in the present work, uniform release of Ti from the chloride ligands leads to formation of rutile phase. Further, the Cl: Ti ratio in Ti-HCl solution determines the crystalline phase. The nucleation and growth of NRs is a very sensitive and complex process. Therefore, in order to understand the growth conditions of NRs on seed layer substrate, the different thicknesses of seed layers have been used to grown NRs at different temperature. $TiO_2$ NRs did not grow on the seed layer coated glass substrate when the temperature was less than 100 ºC which is in good agreement with the rutile $TiO_2$ NRs grown on FTO substrate.[31] The uniform low thickness (~30 nm) seed layer was optimized by spin coating. When decreasing thickness of seed layer by means of decreasing molar concentration in the

solution as well as RPM (rotation per minute) in spin coating, we did not obtain NRs growth on there. Further, it was found that the as-grown NRs at growth temperature 120 ºC – 180 ºC begin to peel off from the substrate, when the thickness of chemical spray pyrolysis coated nuclei layer greater than 150 nm. The peeling of the film could be attributed to the competition between crystal growth and dissolution. The crystal dissolution on high – energy surfaces such as seed – nanorod surface is depends on the reaction time and supersaturation of the Ti salt. At constant Ti concentration, the growth temperature (120 – 180 ºC) and nuclei layer thickness produce strain in interface between nuclei and NRs due to lattice mismatch between them. Owing to this reason, at equilibrium, the rest of the NRs are dissolved in reactant solution. The nuclei layer remain reflecting colors after the $TiO_2$ NRs lifted off from the nuclei layer coated glass substrate, which indicate that the film is peeling off at the seed – nanorod interface.

Generally, four-facets of $TiO_2$ 1D nanostructure generated from 2D nanostructures, therefore, it is possible to investigate different crystallographic plane growth of rutile $TiO_2$ NRs by low thickness of seed layer (~30 nm) subject to NRs growth at higher temperature as well as high thickness of seed layer examined to NRs growth at lower temperature. The reason is thickness of the seed layer decide lattice mismatch with rutile $TiO_2$ and generate different crystallographic plane growth with respect to growth temperature. According to our structural analysis, we propose the two anisotropic crystallographic planes growth of rutile $TiO_2$ NRs along the c - axis. Compare with other surfaces, the (110) face contained Ti and O atomic layer have most stable surface because the growth of rutile $TiO_2$ NRs follows the sequence (110) < (100) < (101) < (001).[45,46] Therefore, at solution temperature 180 ºC, the fast growth rate induces (110) crystallographic plane onto low thickness seed layer due to its surface energy, where each Ti atom is coordinated to the six neighboring O via two apical and four equatorial bonds, resulting

in the randomly oriented lengthy rutile $TiO_2$ NRs. On the other hand, the growth temperature 120 ºC induces (101) crystallographic plane, this promoting the number dense rutile $TiO_2$ NRs on high thickness seed layer. The schematic diagram of the $TiO_2$ NRs growth direction is shown in Fig. 9. To control the growth temperature, the randomly aligned 1D $TiO_2$ NRs grown on different thickness of seed layer substrates are highly reproducible under the identical conditions.

The preferentially oriented crystallographic (110) and (101) plane of rutile $TiO_2$ NRs consisting of three atomic planes, each are repeated along the direction of stacking which is marginally inclined from the normal to the seed layer coated glass substrate.[36] This implies that a dipole moment of atomic planes along the growth direction is zero results in the natural anisotropic growth tendency of $TiO_2$ crystallites. Basically, the crystal growth orientation and morphology of the 1D nanocrystal can be controlled by the basic organic chemistry. Our experimental results reveal that the tetragonal in shape with square top facets of the NRs does not change via free solvent-surface interactions such as hydrogen-bonding, electrostatic and van der Waals interaction. Here, nuclei size of anatase seed layer can selectively determine the (110) and (101) crystallographic plane growth orientation by suppressing further growth of this plane under different growth temperatures, resulting in the number dense and lengthy NRs. From our research work, we conclude that the thickness of seed layer and growth temperature can play a crucial role on the growth rates of different crystal faces and thus provides a useful tool for obtaining $TiO_2$ NRs with number dense and lengthy. The large size and number dense good quality 1 D $TiO_2$ NRs are mandatorily needed for the application of nanostructures anode in photoelectrochemical cells and dye (or) quantum dot sensitized solar cells.

## 5. Conclusions

In summary, we have successfully investigated low and high thickness of nuclei layer on glass substrate for growing 1D $TiO_2$ NRs by spin coating and chemical spray pyrolysis. The well quality $TiO_2$ NRs have grown on $TiO_2$ seed layer coated glass substrate with random alignment by hydrothermal synthesis. The structural investigations reveal the two anisotropic crystallographic planes of tetragonal rutile $TiO_2$ NRs along c-axis. The preferentially oriented (110) and (101) crystallographic plane implies that the $TiO_2$ NRs standing randomly on the seed layer coated glass substrate. Single crystalline nature and growth orientation of the $TiO_2$ NRs are confirmed by HRTEM and SAED pattern. Further, the single crystalline rutile $TiO_2$ NRs is confirmed by micro-Raman measurement. The light scattering effect of charge carrier of $TiO_2$ NRs is explained by using UV-vis absorption spectra. The presence of voids in nuclei layer films confirmed by AFM and then it is staying after NRs growth. Hence, from PL spectra, the excitation photons travel through the air gap between the randomly aligned $TiO_2$ NRs and interact with seed substrate voids to generate SOVs.

**Acknowledgements**

This work was financially supported by the Department of Science and Technology (DST) through Promote University Research for Scientific Excellence (PURSE) scheme. The authors acknowledge UGC-UPE for providing μ-Raman and TEM facilities. Further, the authors also acknowledge the DST-FIST program of School of Physics, Madurai Kamaraj University for provided XRD facility.

**References**

[1]. A. Nakajima, K. Hashimotio, T. Watanabe, K. Takai, G. Yamauchi, A. Fujishima. Langmuir. 16 (2000) 7044.

[2]. K. Guan. Surf. Coat. Technol. 191 (2005) 155.

[3]. A. Fujishima, T. N. Rao, D. A. Tryk. J. Photochem. Photobiol. C. 1 (2000) 1.

[4]. A. L. Linsebigler, G. Lu, J. T. Yates. Jr. Chem. Rev. 95 (1995) 735.

[5]. M. R. Hoffman, S. T. Martin, W. Choi, D. W. Bahnemann. Chem. Rev. 95 (1995) 69.

[6]. P. K. Santra, P. K. Kamat. J. Am. Chem. Soc. 134 (2012) 2508.

[7]. M. K. Nazeeruddin, F. D. Angelis, S. Fantacci, A. Selloni, G. Viscardi, P. Liska, S. Ito, B. Takeru, M. Gratzel. J. Am. Chem. Soc. 127 (2005) 16835.

[8]. P. Soundarrajan. K. Sankarasubramanian, T. Logu, K. Sethuraman, K. Ramamurthi. Mater. Lett. 116 (2014) 191.

[9]. J. Jiu, S. Isoda, F. Wang, M. Adachi. J. Phys. Chem. B. 110 (2006) 2087.

[10]. V. Manthina, J. P. Correa Baena, G. Liu, A. G. Agrios, J. Phys. Chem. C. 116 (2012) 23864.

[11]. Y. X. Zhang, G. H. Li, Y. X. Jin, Y. Zhang, J. Zhang, L. D. Znang. Chem. Phys. Lett. 365 (2002) 300.

[12]. J. Li, W. Wan, H. Zhou, J. Li, P. Xu. Chem. Commun. 47 (2011) 3439.

[13]. X. F. Gao, W. T. Sun, Z. D. Hu, G. Ai, Y. L. Zhang, S. Feng, F. Li, L. M. Peng. J. Phys. Chem. C. 113 (2009) 20481.

[14]. Q. Zheng, G. Chen, Y. Yeng, X. Shen, Y. Zhang, C. Li, R. Yu, Y. Luo, D. Li, Q. Meng. Phys. Chem. Chem. Phys. 14 (2012) 6479.

[15]. W. Zhang, J. Yang, Y. Luo, S. Monti, V. Carravetta. J. Chem. Phys. 129 (2008) 064703.

[16]. H. Perron, J. Vanden borre, C. Domain, R. Drot, J. Roques, E. Simoni, J. J. Ehrhardt, H. Catalette. Surf. Sci. 601 (2007) 518.

[17]. H. Irie, S. Washizuka, K. Hashimota. Thin Solid Films. 21 (2006) 510.

[18]. A.Monoy, A. Brevet, L. Imhoff, B. Domenichini, E, Lesnieswska, P. M. Peterle, M. C. Macro de lucas, S. Bourgeois. Thin Solid Films. 515 (2006) 687.

[19]. L. Kavan, M. Gratzel. Electrochim. Acta. 40 (1995) 643.

[20]. Y. Lei, L. D. Zhang, J. C. Fan. Chem. Phys. Lett. 338 (2001) 231.

[21]. Y. A. Cao, J. N. Yao, J. Znang, T. D. Hu. Langmuir. 19 (2003) 3001.

[22]. K. Pomoni, A. Vomvas, Chr. Trapalis. Thin Solid Films. 479 (2005) 160.

[23]. I. Oja, A. Mere, M. Krunks, R. Nisumaa, C. H. Solterbeck, M. Es-Souni. Thin. Solid. Films. 515 (2006) 674.

[24]. X. Zhao, M. Liu, Y. Zhu. Thin. Solid. Films. 515 (2007) 7127.

[25]. W. Yang, F. Wan, S. Chen, C. Jiang. Nanoscale. Res. Lett. 4 (2009) 1486.

[26]. C. Wang, Z. Jiang, L. Wei, Y. Chen, J. Jiao, M. Eastman, H. Liu. Nano Energy. 1 (2012) 440.

[27]. H. Wang, Y. Bai, H. Zhang, Z. Zhang, J. Li, L. Guo. J. Phys. Chem. C. 114 (2010) 16451.

[28]. V. Tamilselvan, D. Yuvaraj, R. Rakesh Kumar, K. Narasimha Rao. Appl. Surf. Sci. 258 (2012) 4283.

[29]. A. Wolcott, W. A. Smith, T. R. Kuykendall, Y. Zhao, J. Z. Zhange. Small. 5 (2009) 104.

[30]. J. T. Park, R. Patel, H. Jeon, D. J. Kim, J. S. Shin, J. H. Kim. J. Mater. Chem. 22 (2012) 6131.

[31]. B. Liu, E. S. Aydil. J. Am. Chem. Soc. 131 (2009) 3985.

[32]. F. Zheng, M. Guo, M. Zheng. Cryst. Eng. Comm. 15 (2013) 277.

[33]. P. I. Gouma, M.J. Mills. J. Am. Ceram. Soc. 84 (2001) 619.

[34]. W. Ma, Z. Lu, M. Zhang. Appl. Phys. 66 (1998) 621.

[35]. H. Z. Zhang, J.F. Banfied. J. Mater. Res. 15 (2000) 437.

[36]. R. A. Evarestov, Y.F. Zhukovskii. Surf. Sci. 608 (2013) 226.

[37]. Q. Tang, W. Zhou, J. Shen, W. Zhange, L. Kong, Y. Qian. Chem. Commun. (2004) 712.

[38]. G. M. Begun, C. E. Bamberger. Appl. Spectrosc. 43 (1989) 134.

[39]. W. Wang, B. Gu, L. Liang, W. A. Hamilton, D. J. Wesolowski. J. Phys. Chem. B. 108 (2004) 1489.

[40]. S.P.S. Porto, P.A. Fleury, T.C. Damen. Phys. Rev. 154 (1967) 522.

[41]. A.V. Korotcov, Y.S. Huang, K.K. Tiong, D.S. Tsai. J. Raman Spectrosc. 38 (2007) 737.

[42]. F. Rossella, P. Galinetto, M. C. Mozzati, L. Malavasi, Y. Diaz Fernandez, G. Drera, L. Sangaletti. J. Raman Spectrosc. 41 (2010) 558.

[43]. S. S. Amin, A. W. Nicholls, T. T. Xu. Nanotechnology. 18 (2007) 445609.

[44]. S.A. Berhe, S. Nag, Z. Molinets, W.J. Youngblood. Appl. Mater. Interfaces. 5 (2013) 1181.

[45]. E. Hosono, S. Fujihara, K. Kakiuchi, H. Imai. J. Am. Chem. Soc. 126 (2004) 7790.

[46]. X. Wu, Z. Chen, G. Q. Lu, L. Wang. Adv. Funct. Mater. 21 (2011) 4166.

**Figure captions**

Flg 1. XRD patterns of the $a_1$ and $b_1$ NRs.

Fig 2. TEM, HRTEM and SAED patterns of the $a_1$ and $b_1$ NRs.

Fig 3. Different magnification SEM images of $a_1$ and $b_1$ NRs and ($a_2$, $b_2$) corresponding NRs square top distributions.

Fig 4. EDAX spectrum of $a_1$ sample.

Fig 5. AFM images of (a, b) $TiO_2$ seed layer and ($a_1$, $b_1$) as-grown $TiO_2$ NRs.

Fig 6. (i) Absorption spectra of (a, b) $TiO_2$ seed layers and ($a_1$, $b_1$) NRs. (ii) Band gap energy values of (a, b) $TiO_2$ seed layers and ($a_1$, $b_1$) NRs.

Fig 7. (i) Photoluminescence spectra of ($a_1$, $b_1$) NRs and (ii) FTIR spectra of ($a_1$, $b_1$) $TiO_2$ NRs.

Fig 8. micro-Raman spectrum of $a_1$ and $b_1$ NRs.

Fig 9. Schematic diagram of (110) and (101) growth habit of rutile $TiO_2$ NRs.

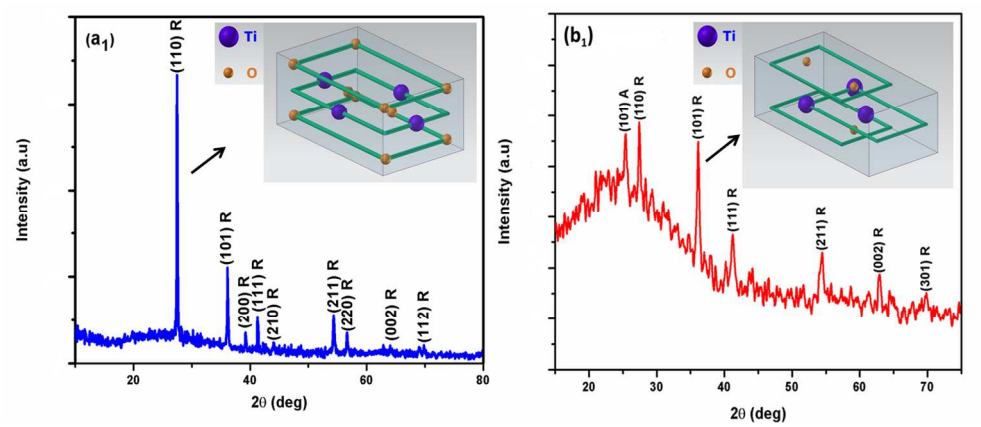


406x170mm (96 x 96 DPI)

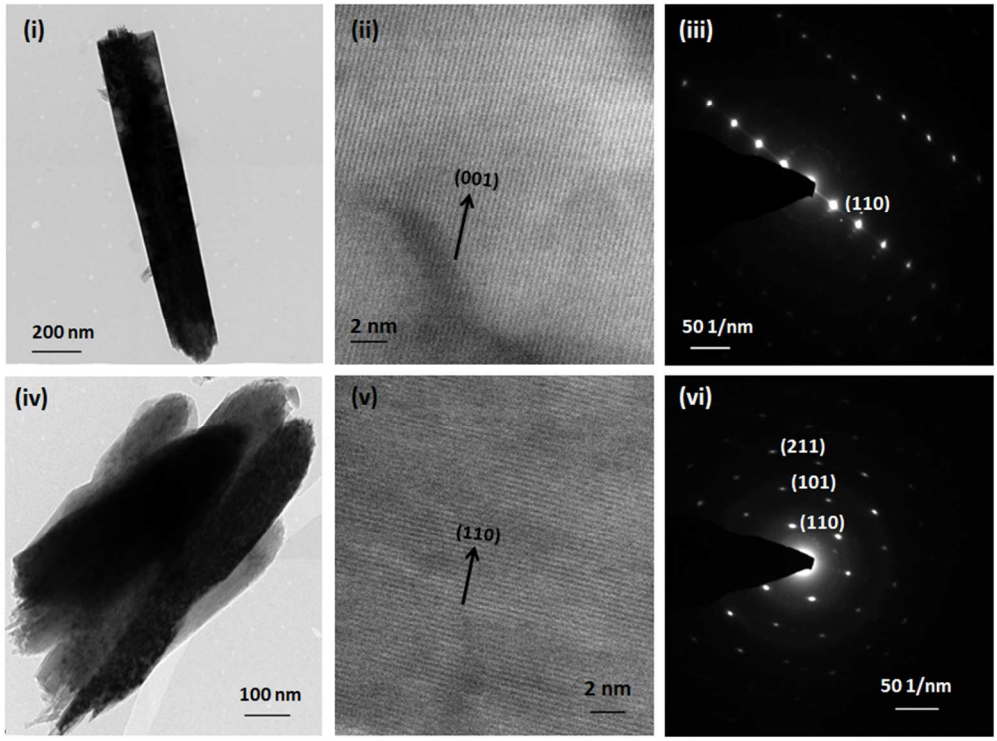


245x183mm (96 x 96 DPI)

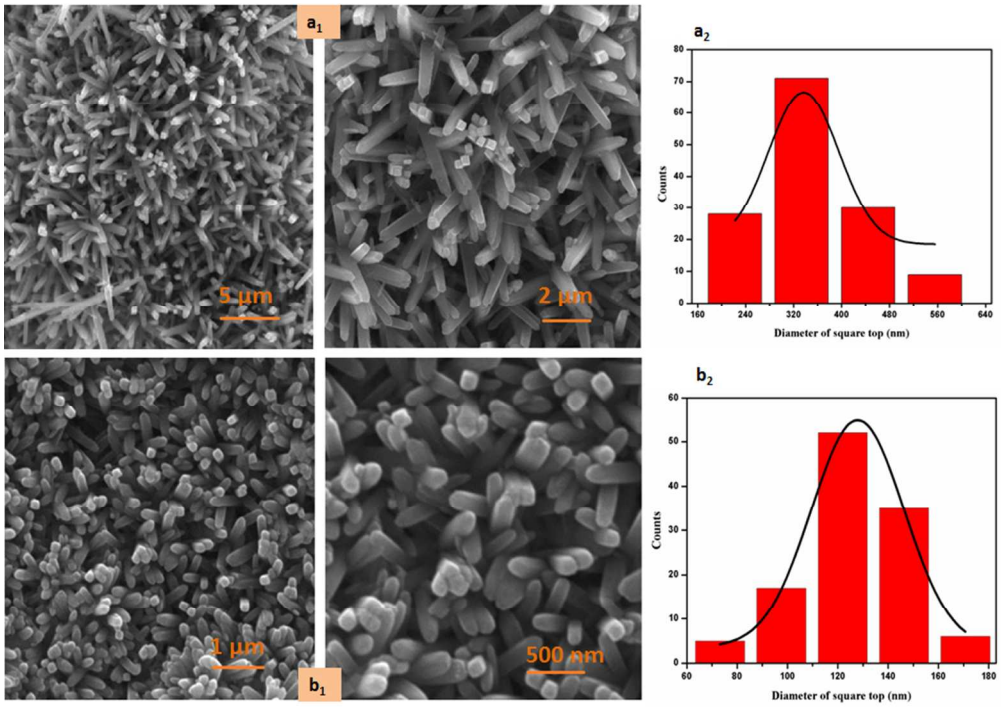


251x177mm (96 x 96 DPI)

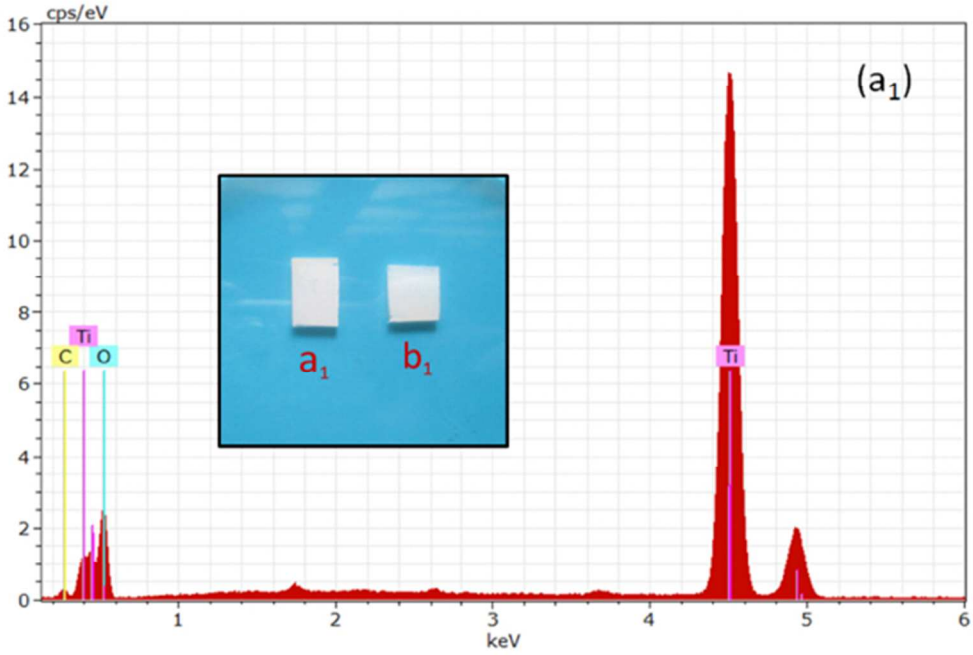


251x165mm (70 x 71 DPI)

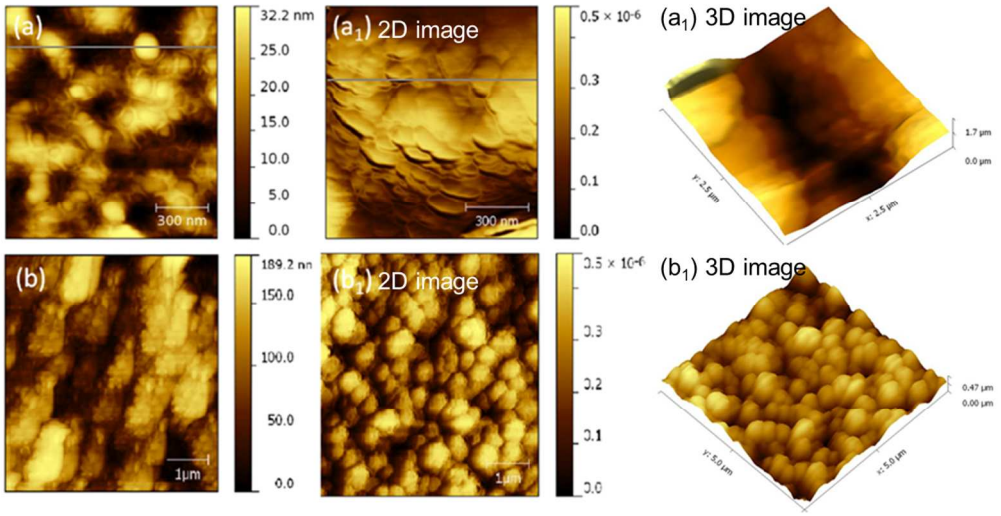


232x120mm (150 x 150 DPI)

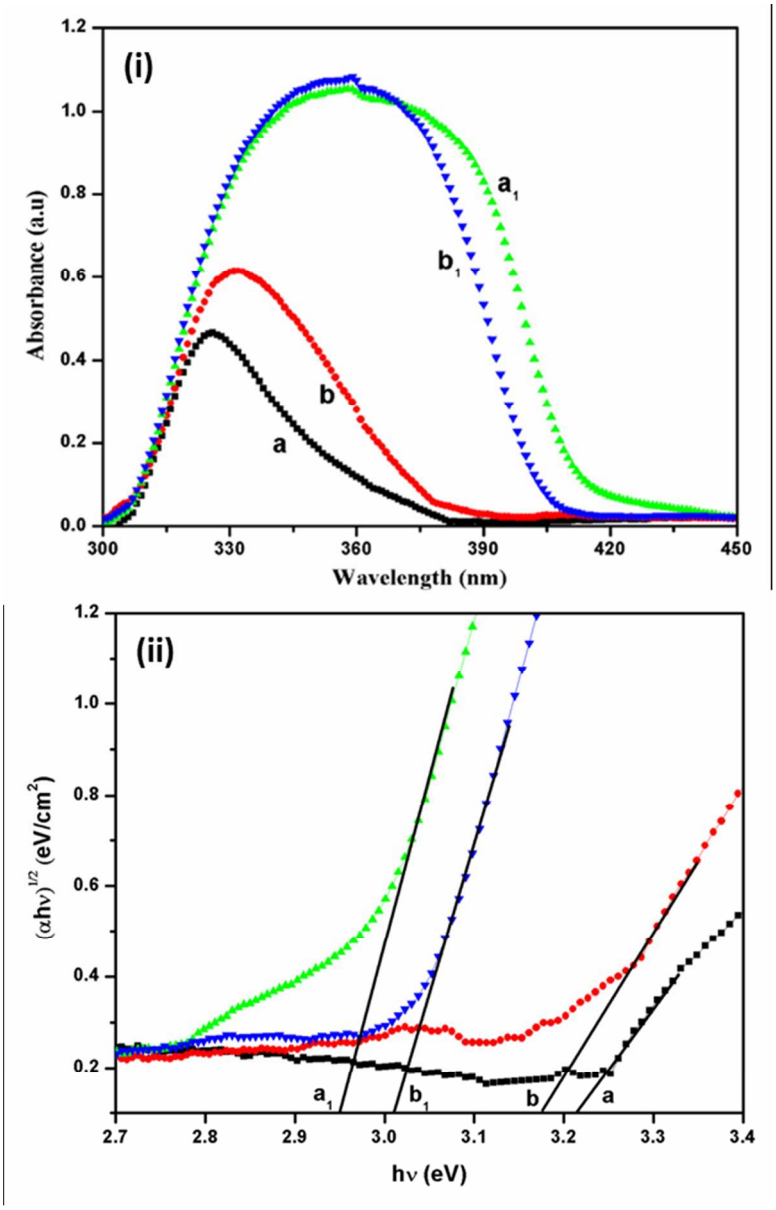


105x165mm (150 x 150 DPI)

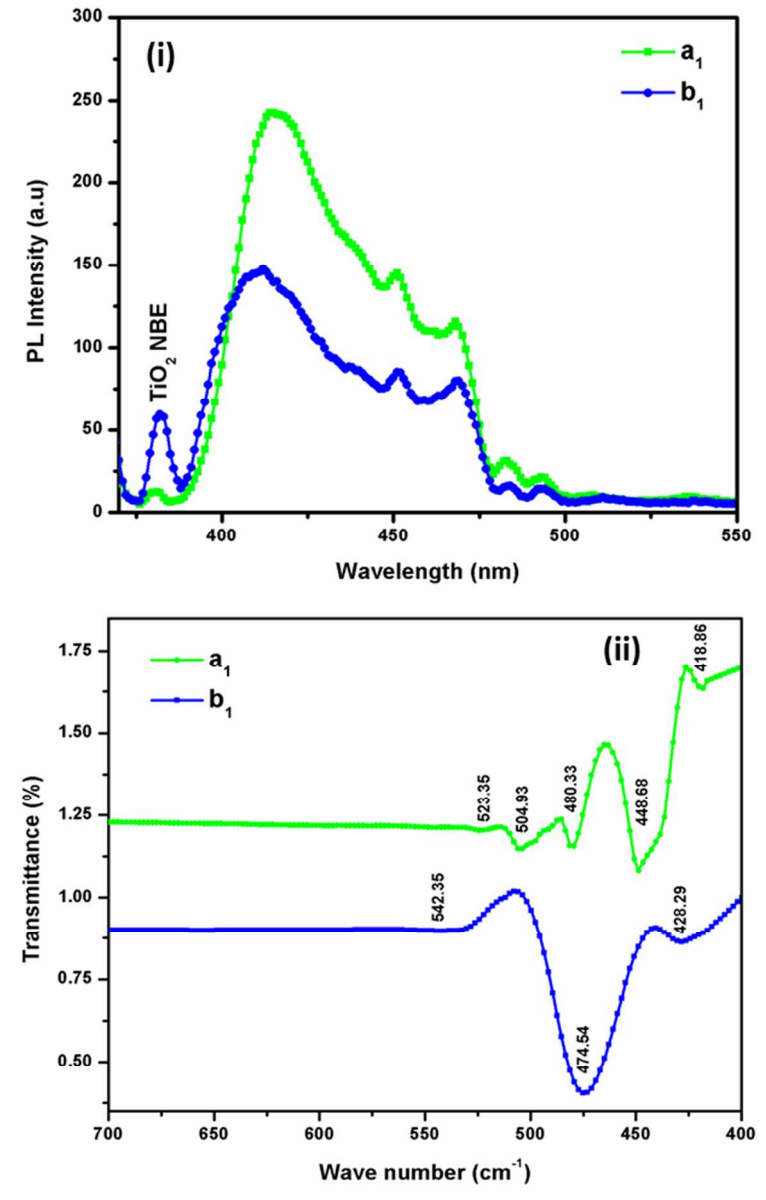


108x167mm (150 x 150 DPI)

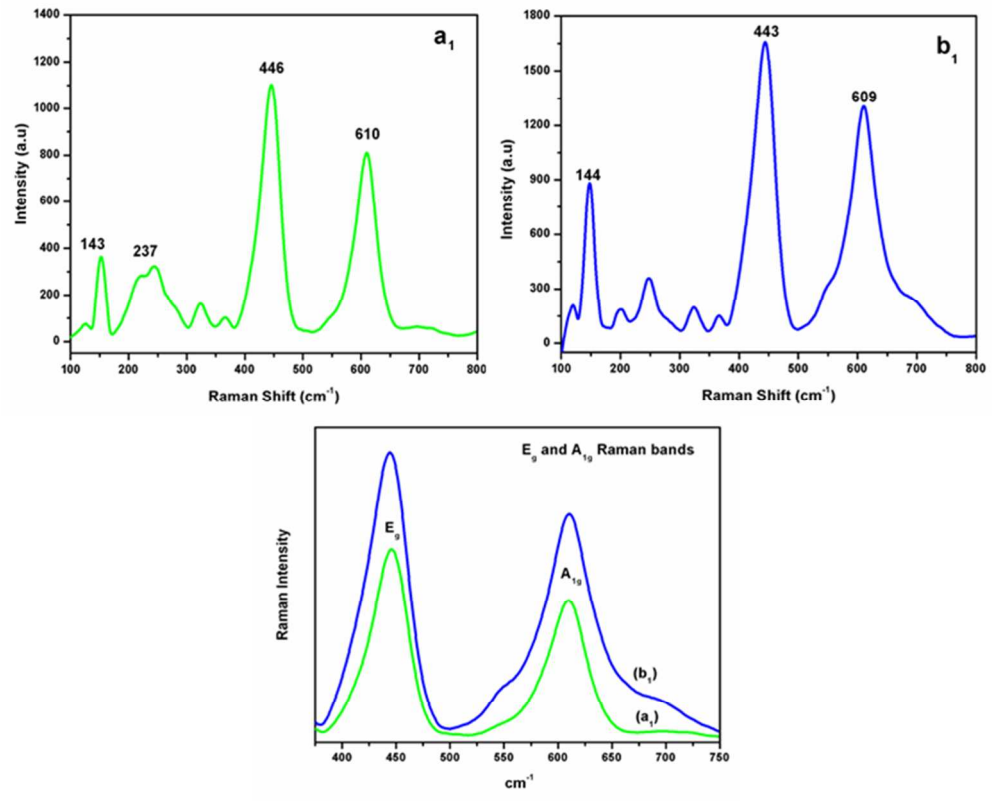


228x183mm (92 x 92 DPI)

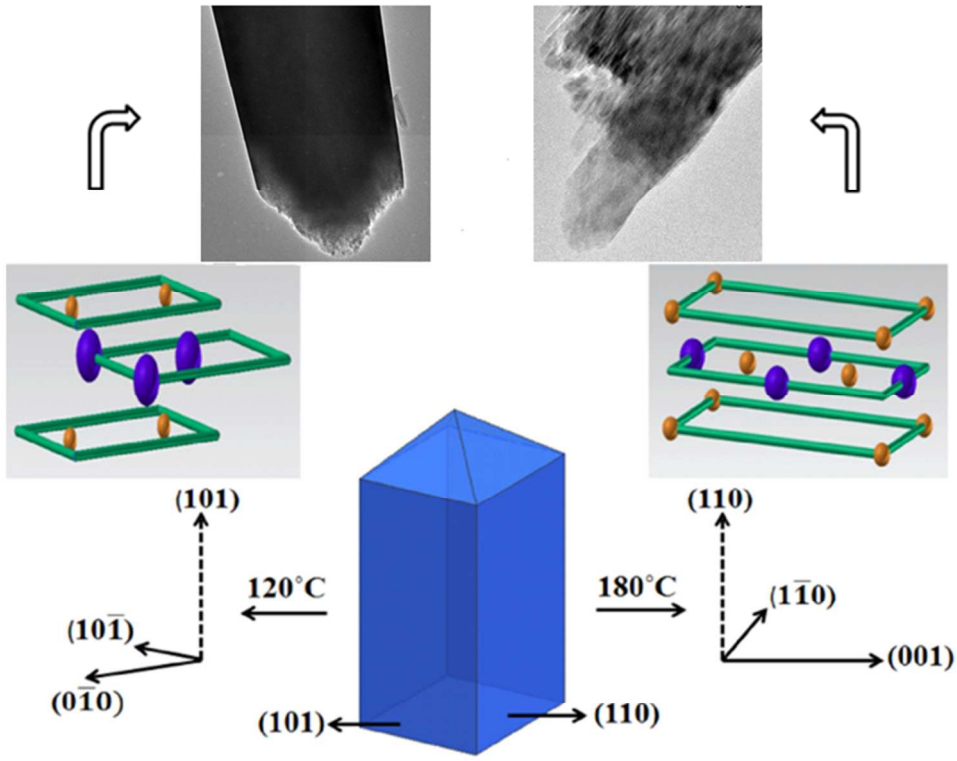


227x186mm (99 x 99 DPI)